IPEM Institute of Physics and Engineering in Medicine

PAPER

Synchronous behaviour in network model based on human cortico-cortical connections

To cite this article: P R Protachevicz *et al* 2018 *Physiol. Meas.* **39** 074006

View the article online for updates and enhancements.

Related content

- Synchronization of the SWNN with unreliable synapses
Chunguang Li and Qunxian Zheng

- Impact of type of intracranial EEG sensors on link strengths of evolving functional brain networks
Ancor Sanz-Garcia, Thorsten Rings and Klaus Lehnertz

- Criticality in the brain
L de Arcangelis, F Lombardi and H J Herrmann

Physiological Measurement

IPEM Institute of Physics and Engineering in Medicine

Synchronous behaviour in network model based on human cortico-cortical connections

P R Protachevicz[1], R R Borges[2], A S Reis[3], F S Borges[4], K C Iarosz[5,6,7], I L Caldas[5], E L Lameu[7,8], E E N Macau[8,9], R L Viana[3], I M Sokolov[7], F A S Ferrari[10], J Kurths[6,7], A M Batista[1,6,11], C-Y Lo[12], Y He[13,14,15] and C-P Lin[16]

1 Graduation in Science Program-Physics, State University of Ponta Grossa, Ponta Grossa, PR, Brazil
2 Department of Mathematics, Federal University of Technology-Paraná, Apucarana, PR, Brazil
3 Department of Physics, Federal University of Paraná, Curitiba, PR, Brazil
4 Center for Mathematics, Computation, and Cognition, Federal University of ABC, São Bernardo do Campo, SP, Brazil
5 Institute of Physics, University of São Paulo, São Paulo, SP, Brazil
6 Potsdam Institute for Climate Impact Research, Potsdam, Germany
7 Department of Physics, Humboldt University of Berlin, Berlin, Germany
8 National Institute for Space Research, São José dos Campos, SP, Brazil
9 Federal University of São Paulo, São José dos Campos, SP, Brazil
10 Institute of Engineering, Science and Technology, Federal University of Vales do Jequitinhonha e Macuri, Janaúba, MG, Brazil
11 Department of Mathematics and Statistics, State University of Ponta Grossa, Ponta Grossa, PR, Brazil
12 Institute of Science and Technology for Brain-Inspired Intelligence, Fudan University, Shanghai, People's Republic of China
13 National Key Laboratory of Cognitive Neuroscience and Learning, Beijing Normal University, Beijing, People's Republic of China
14 Beijing Key Laboratory of Brain Imaging and Connectomics, Beijing Normal University, Beijing, People's Republic of China
15 IDG/McGovern Institute for Brain Research, Beijing Normal University, Beijing, People's Republic of China
16 Institute of Neuroscience, National Yang-Ming University, Taipei, Taiwan

E-mail: kiarosz@gmail.com

Abstract

Objective: We consider a network topology according to the cortico-cortical connection network of the human brain, where each cortical area is composed of a random network of adaptive exponential integrate-and-fire neurons. *Approach*: Depending on the parameters, this neuron model can exhibit spike or burst patterns. As a diagnostic tool to identify spike and burst patterns we utilise the coefficient of variation of the neuronal inter-spike interval. *Main results*: In our neuronal network, we verify the existence of spike and burst synchronisation in different cortical areas. *Significance*: Our simulations show that the network arrangement, i.e. its rich-club organisation, plays an important role in the transition of the areas from desynchronous to synchronous behaviours.

1. Introduction

The brain is the most complex organ in the human body (Bullmore and Sporns 2009). The cerebral cortex is the brain region with the biggest superficial area and plays a key role in consciousness, memory, perception, thought, and cognition (Shaw *et al* 2008). It is interconnected by a network of cortico-cortical axonal pathways (Hagmann *et al* 2008). In the cortico-cortical connections, axons transmit excitatory stimulii from one cortical area to another (Ottersen and Storm-Mathisen 1986).

Brain network interactions can be analysed by means of a framework from the new interdisciplinary field of network physiology (Bashan *et al* 2012). Network physiology allows one to identify the relations between physiological function and network topology (Ivanov and Bartsch 2014). The brain has communication channels with other organs, such as the channel of communication for brain–heart interactions (Ivanov *et al* 2016). Bartsch *et al* (2015) showed networked interactions within and across brain hemispheres. Liu *et al* (2015) found interactions between physiologic states and network structure. They reported new aspects of functional plasticity as a consequence of brainwave interactions across the brain during different physiologic states.

In the brain, there is much experimental evidence of neuronal synchronisation, where the synchronous behaviour is related to the execution of several tasks (Tallon-Baudry 2009). When there are interactions among oscillatory activities of action potentials they adjust their phases and frequencies and can exhibit neuronal syn-

chronisation (Erra *et al* 2017). According to Pikovsky *et al* (2001), synchronisation manifests itself via frequency and phase locking. Synchronisation of neuronal activity is involved in brain mechanisms such as perception (Rodriguez *et al* 1999) and memory processes (Fell and Axmacher 2011). However, certain brain disorders are associated with neuronal synchronisation (Uhlhass and Singer 2006). Parkinson's disease is associated with synchronised oscillatory activity (Brown 2003, Andres *et al* 2014). Epilepsy is characterised by an increase of synchronous neuronal activity that happens in the majority of neurons in a local area (Traub and Wong 1982).

There are many ways in which one can build neuronal networks to study synchronisation. In the literature, mathematical models of various kinds of networks have been considered to simulate synchronous behaviours, for instance coupled Kuramoto-like phase oscillators (Zhang *et al* 2014, 2015). Different network topology and model parameters can lead different paths to synchronisation on network systems (Gómez-Gardeñes *et al* 2007). In this work, we study synchronisation in a network with neurons connected according to the cortico-cortical connection network constructed by Lo *et al* (2010). They used diffusion tensor image tractography to build human brain networks of healthy patients. The structural network was separated into 78 cortical areas. We consider a subnetwork in each cortical area, where the subnetwork connections are randomly distributed. Each neuron is described by the adaptive exponential integrate-and-fire model (aEIF) (Brette and Gerstner 2005). The aEIF model reproduces electrophysiological characteristics of neurons and its parameters have a physiological interpretation (Touboul and Brette 2008). Depending on the parameter values, it is possible to observe multiple firing patterns and transition from one firing type to another (Naud *et al* 2008). Borges *et al* (2017) studied firing patterns in a random network of aEIF. They analysed how spike or burst synchronous behaviour appears as a function of the coupling strength and the probability of connections.

In our neuronal network, we observe the coexistence of different firing patterns, namely some cortical areas exhibiting spike and others burst behaviours at the same time (Connors and Gutnick 1990). We also observe spike and burst synchronous behaviours in the network. We verify that there are areas with synchronous behaviour embedded in the desynchronised network. It is shown that the transition of the areas from desynchronous to synchronous patterns is related to the rich-club organisation of our neuronal network. There is experimental evidence that some brain regions form a rich-club (van den Heuvel and Sporns 2011). A rich-club is a group of neurons with more connections than others.

This paper is organised as follows. In section 2, we present the adaptive exponential integrate-and-fire model and introduce the neuronal network. In section 3, we study the spike and burst synchronisation. In the last section, we draw our conclusions.

2. Neuronal network of aEIF

In this section we introduce the considered model for a neuron, namely the adaptive exponential integrate-and-fire (aEIF), given by Brette and Gerstner (2005):

$$C\frac{dV}{dt} = -g_L(V - E_L) + g_L\Delta_T\exp\left(\frac{V - V_T}{\Delta_T}\right) + I - \mu, \tag{1}$$

$$\tau_\mu\frac{d\mu}{dt} = a(V - E_L) - \mu, \tag{2}$$

where C is the membrane capacitance, V is the membrane potential, I is the injected current, g_L is the leak conductance, E_L is the resting potential, Δ_T is the slope factor, V_T is the threshold potential, μ is the adaptation variable, τ_μ is the time constant, and a is the level of subthreshold adaptation. A reset condition is applied when V arrives at a threshold V_{peak}: $V = V_r$ and $\mu = \mu_r = \mu + b$. We use in our simulations $C = 200$ pF, $g_L = 12$ nS, $E_L = -70$ mV, $\Delta_T = 2$ mV, $V_T = -50$ mV, $I = 509.7$ pA, $\tau_\mu = 300$ ms, $a = 2$ nS, $V_r = -60$ mV and $V_{peak} = 20$ mV (Naud *et al* 2008).

We utilise the coefficient of variation (CV) of the neuronal inter-spike interval (ISI) as a diagnostic tool to identify spike and burst patterns, that is given by

$$CV = \frac{\sigma_{ISI}}{M_{ISI}}, \tag{3}$$

where σ_{ISI} corresponds to the standard deviation of the ISI normalised by the mean M_{ISI} (Gabbiani and Koch 1998). Spike and burst patterns have CV < 0.5 and CV ⩾ 0.5, respectively. In our simulations, we verify that the threshold value of CV equal to 0.5 is enough to separate the patterns into spike and burst. Figure 1 shows the temporal evolution of the membrane potential of the aEIF neuron. Figures 1(a) and (b) show spikes (CV ≈ 0.05) and bursts (CV ≈ 0.8), respectively.

We built a neuronal network according to the cortico-cortical connection network of the human brain obtained by Lo *et al* (2010). These authors determined the nodes of brain networks by means of an automated anatomical labeling template, and the edges were determined using diffusion magnetic resonance imaging trac-
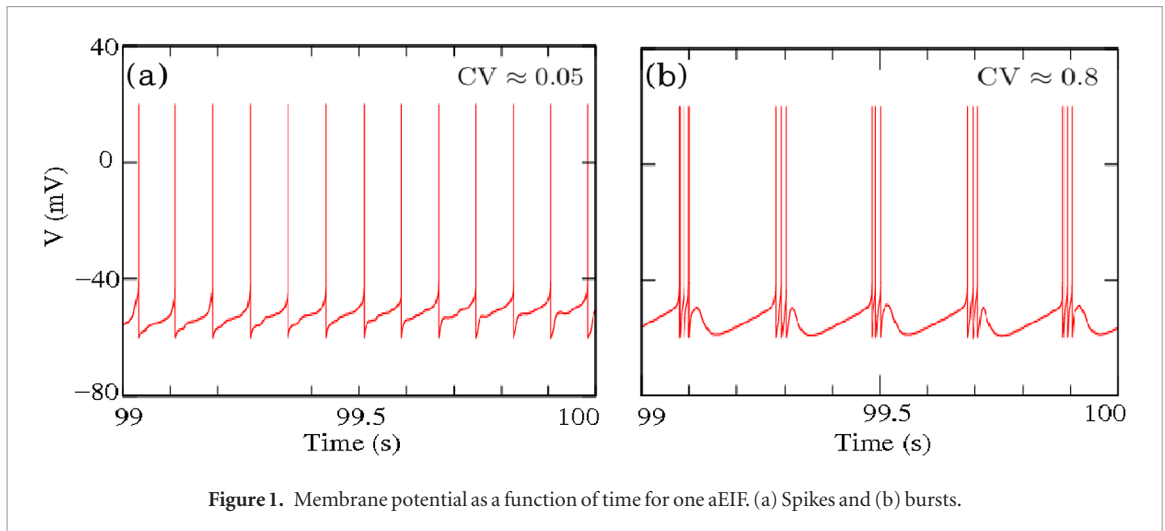
Figure 1. Membrane potential as a function of time for one aEIF. (a) Spikes and (b) bursts.
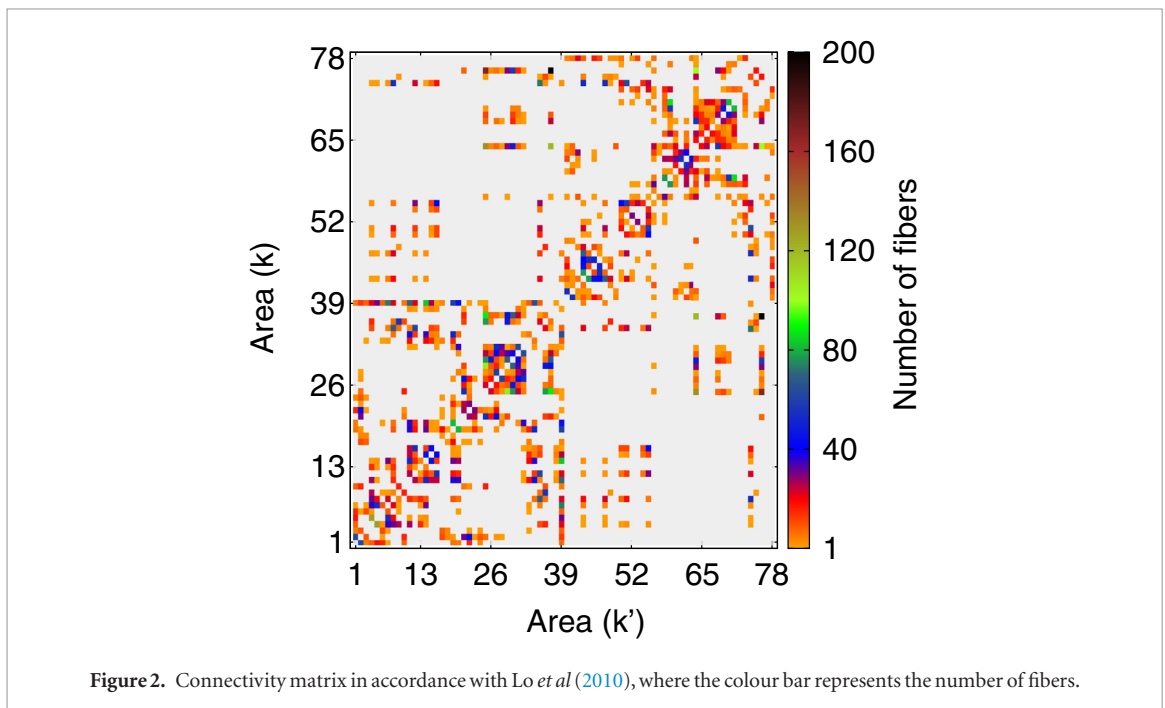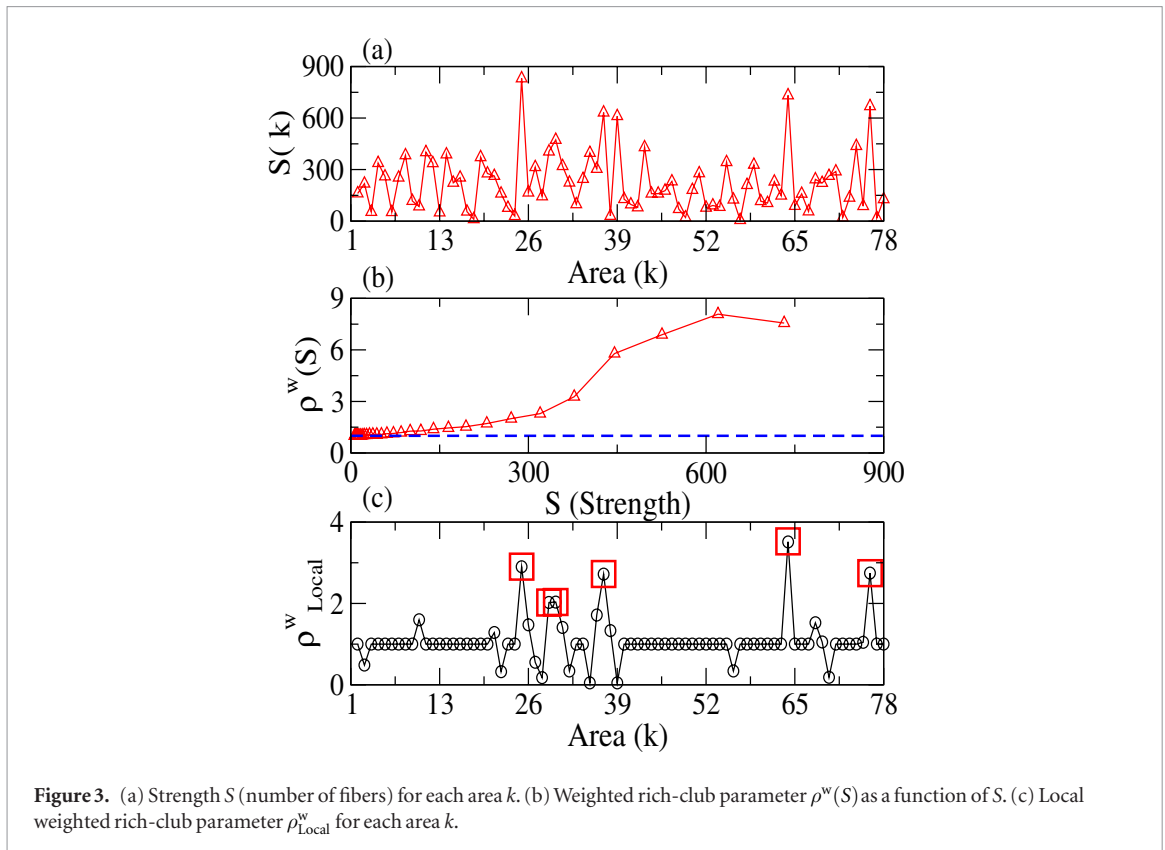

Figure 2. Connectivity matrix in accordance with Lo *et al* (2010), where the colour bar represents the number of fibers.

tography methods. The fibers tracking was performed though fiber assignment by a continuous tracking algorithm. Figure 2 displays the 78 cortical areas and the number of detected fibers (connections) between them in the human brain. The colours represent the number of fibers. In our simulations, we consider that one fiber corresponds to one connection.

Rich-club organisation is characterised by a tendency of highly connected neurons of the network to be very well-connected to each other. In order to examine the connectivity profile of the network we use the weighted rich-club parameter (Colizza *et al* 2006, Opsahl *et al* 2008)

$$\phi^{\mathrm{w}}(r) = \frac{W_{>r}}{\sum_{l=1}^{E_{>r}} \mathrm{w}_l^{\mathrm{rank}}}, \qquad (4)$$

where r is the richness index obtained from the sum of the weights attached to the connections originating from a neuron, $\mathrm{w}_l^{\mathrm{rank}} \geqslant \mathrm{w}_{l+1}^{\mathrm{rank}}$ ($l = 1, 2, ..., E$) are the ranked weights on the connections of the network, and E is the total number of connections. For each r value is selected a set (club) of nodes with a richness index larger than r. $E_{>r}$ is the number of connections between the rich club members, and $W_{>r}$ is the sum of the weights associated with these connections. Therefore, $\phi^{\mathrm{w}}(r)$ is the ratio between $W_{>r}$ and the sum of the weights attached to the strongest connections $E_{>r}$ within the whole network. However, $\phi^{\mathrm{w}}(r)$ is not sufficient to characterise the rich-club due to the fact that networks with random connections can have a non-zero $\phi^{\mathrm{w}}(r)$ value. Then, to identify the rich-club we calculate the ratio

Figure 3. (a) Strength S (number of fibers) for each area k. (b) Weighted rich-club parameter $\rho^{\mathrm{w}}(S)$ as a function of S. (c) Local weighted rich-club parameter $\rho^{\mathrm{w}}_{\mathrm{Local}}$ for each area k.

$$\rho^{\mathrm{w}}(r) = \frac{\phi^{\mathrm{w}}(r)}{\phi^{\mathrm{w}}_{\mathrm{Random}}(r)}. \tag{5}$$

When $\rho^{\mathrm{w}}(r) > 1$ over a range of r, there is a rich-club organisation in the network.

Figure 3(a) shows the number of fibers S for each area k. The areas $25, 64, 76, 37$, and 39 have the largest number of fibers (descending order). In figure 3(b), we calculate the weighted rich-club parameter $\rho^{\mathrm{w}}(S)$ as a function of S. We find $\rho^{\mathrm{w}} > 1$ for $S > 100$; as a result, our neuronal network is organised as a rich-club. In addition, the areas $25, 29, 30, 37, 64$, and 76 (red squares) are the most interconnected and have the higher values of $\rho^{\mathrm{w}}_{\mathrm{Local}}$ (local rich-club), as shown in figure 3(c).

For each area we consider a subnetwork with $N_k = 100$ neurons randomly connected with probability $p = 0.4$. This way, the network has a total of $N = 7800$ neurons, and the neuronal dynamics are given by

$$C\frac{dV_i}{dt} = -g_L(V_i - E_L) + g_L\Delta_T\exp\left(\frac{V_i - V_T}{\Delta_T}\right) + I_i - \mu_i$$

$$+ g_{\mathrm{ex}}(V_{\mathrm{ex}} - V_i)\sum_{j=1}^{N_{\mathrm{ex}}} A_{ij}s_j + g_{\mathrm{in}}(V_{\mathrm{in}} - V_i)\sum_{j=1}^{N_{\mathrm{in}}} B_{ij}s_j, \tag{6}$$

$$\tau_\mu \frac{d\mu_i}{dt} = a_i(V_i - E_L) - \mu_i, \tag{7}$$

$$\tau_{\mathrm{s}} \frac{ds_i}{dt} = -s_i, \tag{8}$$

where V_i is the membrane potential of the neuron i, g_{ex} (g_{in}) is the excitatory (inhibitory) synaptic conductance, N_{ex} (N_{in}) is the number of excitatory (inhibitory) neurons, $V_{\mathrm{ex}} = 0$ ($V_{\mathrm{in}} = -80$ ms) is the excitatory (inhibitory) synaptic reversal potential, $\tau_s = 2.728$ ms is the synaptic time constant, s_i is the synaptic weight, and a_i is randomly distributed in the interval $[1.9, 2.1]$ to simulate a network with different neurons. The solution to equation (8) is an exponential decay, where we consider the initial value of the solution $s_i(0) = 0$ and $s_i = s_i + 1$ when the neuron i spikes. A_{ij} and B_{ij} are the excitatory and inhibitory adjacency matrices, respectively. Inside the subnetworks, we randomly distribute 80% of excitatory and 20% of inhibitory connections (Noback *et al* 2005), while the connections among the subnetworks are excitatory.
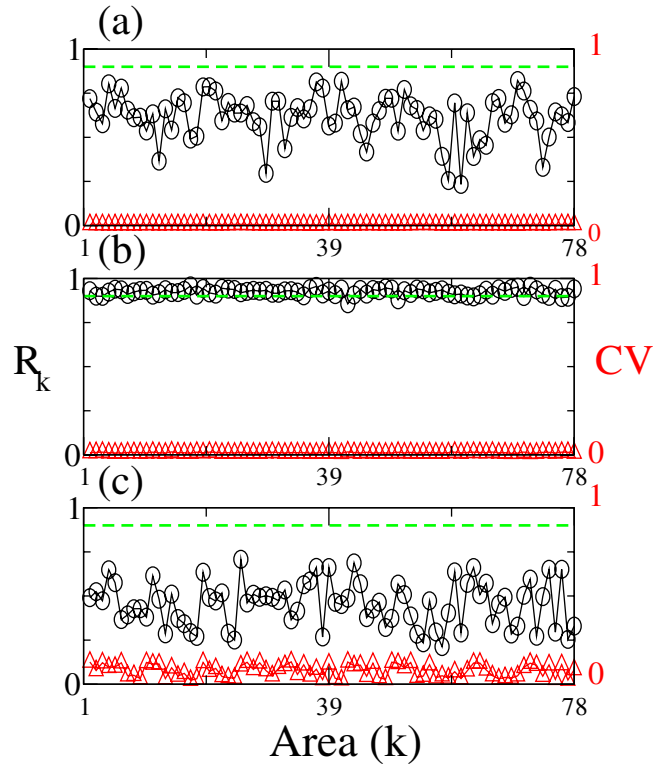
Figure 4. R_k (black circles) and CV (red triangles) for (a) $\varepsilon = 0.05$, (b) $\varepsilon = 0.2$, (c) $\varepsilon = 0.55$, where $\varepsilon = g_{ex} = g_{in}$. We consider that the area is synchronised when the average order parameter value is larger than $R_k = 0.9$ (green line). In all cases spike dynamics are observed (CV < 0.5).

3. Synchronous behaviour

Synchronous behaviour has been found throughout the brain in task and rest conditions (Deco *et al* 2011). We use the complex phase order parameter as a diagnostic tool to identify neuronal synchronisation (Kuramoto 1984) in each area,

$$Z_k(t) = R_k(t) e^{i\psi^{(k)}(t)} = \frac{1}{N_k} \sum_{j=1}^{N_k} e^{i\theta_j^{(k)}(t)}, \tag{9}$$

where

$$\theta_j^{(k)}(t) = 2\pi \frac{t - t_{j,m}}{t_{j,m+1} - t_{j,m}} \tag{10}$$

is the phase of the neuron j in the area k, $1 \leqslant k \leqslant 78$, with $t_{j,m} < t < t_{j,m+1}$, and N_k is the number of neurons of the area k. The time $t_{j,m}$ denotes the mth spike of the neuron j, and $\psi^{(k)}(t)$ is the average phase of all neurons in each subnetwork. The order parameter averaged over the time interval from t_{initial} to t_{final} is given by

$$R_k = \frac{t_{\text{step}}}{t_{\text{final}} - t_{\text{initial}}} \sum_{t_{\text{initial}}}^{t_{\text{final}}} \left| \frac{1}{N_k} \sum_{j=1}^{N_k} e^{i\theta_j^{(k)}(t)} \right| \tag{11}$$

where $t_{\text{initial}} = 80$ s, $t_{\text{final}} = 100$ s, and $t_{\text{step}} = 0.5$ ms. The R_k value is equal to 1 in complete synchronised behaviour. For $R_k \geqslant 0.9$ the network exhibits an intensely synchronised regime.

Figure 4 exhibits the R_k (black circles) and CV (red triangles) for a network with excitatory and inhibitory synapses. For $\varepsilon = 0.05$ ($\varepsilon = g_{ex} = g_{in}$), we see all areas with $R_k < 0.9$ and CV < 0.5 due to the fact that the neurons inside the subnetwork display desynchronised spikes (figure 4(a)). The areas change from desynchronous to synchronous behaviours when ε values are increased to 0.2 (figure 4(b)). As CV < 0.5 for all areas, the subnetworks have a spike pattern. As shown in figure 4(c), considering $\varepsilon = 0.55$ the network changes its behaviour from synchronised to desynchronised spikes (Borges *et al* 2017).

After the transition of all areas to desynchronised spikes, increasing ε, the areas 25, 29, 30, 37, 64, and 76 not only synchronise but also they change from spike to burst patterns before other areas (figure 5(a)). These areas correspond to areas with higher values of $\rho_{\text{Local}}^{\text{w}}$, as shown in figure 3(c). For $\varepsilon = 0.7$ we observe that all areas change to burst synchronisation (figure 5(b)).
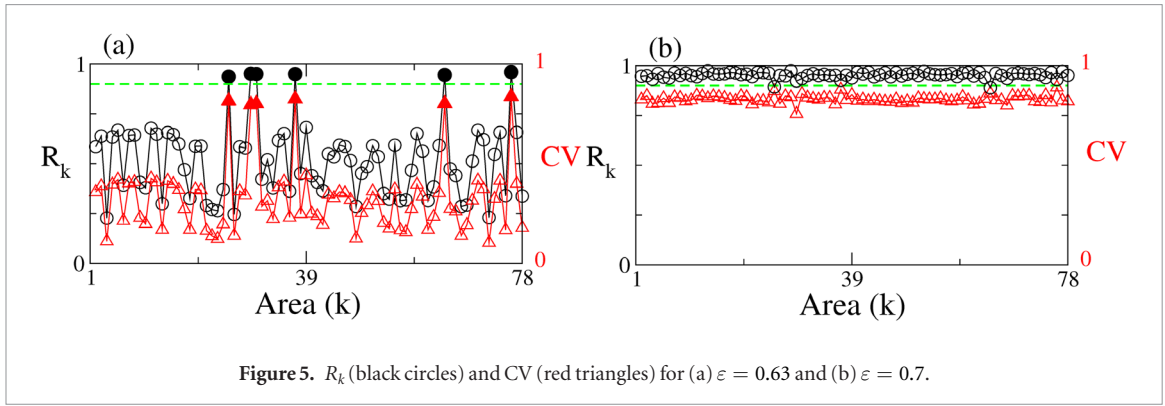
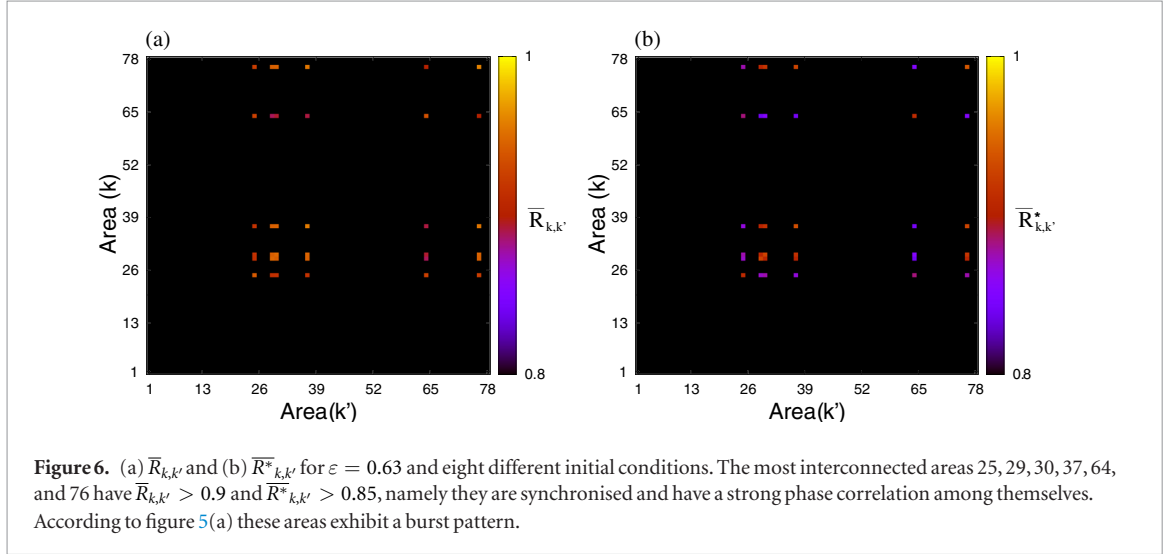**Figure 5.** R_k (black circles) and CV (red triangles) for (a) $\varepsilon = 0.63$ and (b) $\varepsilon = 0.7$.

Figure 6. (a) $\overline{R}_{k,k'}$ and (b) $\overline{R}^*_{k,k'}$ for $\varepsilon = 0.63$ and eight different initial conditions. The most interconnected areas $25, 29, 30, 37, 64$, and 76 have $\overline{R}_{k,k'} > 0.9$ and $\overline{R}^*_{k,k'} > 0.85$, namely they are synchronised and have a strong phase correlation among themselves. According to figure 5(a) these areas exhibit a burst pattern.

In order to identify the synchronisation between areas k and k', we consider the time average order parameter

$$R_{k,k'} = \frac{t_{\text{step}}}{t_{\text{final}} - t_{\text{initial}}} \sum_{t_{\text{initial}}}^{t_{\text{final}}} \left| \frac{1}{N_k + N_{k'}} \left(\sum_{j=1}^{N_k} e^{i\theta_j^{(k)}(t)} + \sum_{j=1}^{N_{k'}} e^{i\theta_j^{(k')}(t)} \right) \right|. \tag{12}$$

The mean of $R_{k,k'}$ for different initial conditions is given by $\overline{R}_{k,k'}$. In figure 6(a), we see that almost all $\overline{R}_{k,k'}$ values are less than 0.9. Nevertheless, the most interconnected areas (25, 29, 30, 37, 64, and 76) exhibit $\overline{R}_{k,k'} > 0.9$ and CV > 0.5 (figure 5(a)), indicating not only synchronised bursts inside the subnetworks but also that these areas are synchronised among themselves. We also calculate the phase correlation $R^*_{k,k'}$ between the areas k and k' by means of the equations

$$R^*_{k,k} = \frac{1}{N_k(N_k - 1)} \sum_{i,j \in k, j \neq i} R_{ij}, \tag{13}$$

when $k = k'$, and

$$R^*_{k,k'} = \frac{1}{N_k N_{k'}} \sum_{i \in k} \sum_{j \in k'} R_{ij}, \tag{14}$$

when $k \neq k'$, where R_{ij} is the local order parameter used to analyse the phase correlation between neurons i and j (Gómez-Gardeñes *et al* 2007, Zhang *et al* 2014),

$$R_{ij} = \frac{t_{\text{step}}}{t_{\text{final}} - t_{\text{initial}}} \sum_{t_{\text{initial}}}^{t_{\text{final}}} \left| e^{i[\theta_i(t) - \theta_j(t)]} \right|. \tag{15}$$

Figure 6(b) shows the mean of $R^*_{k,k'}$, where the average is taken over eight different initial conditions. We verify that the most interconnected areas have a strong phase correlation among themselves.

Next, we calculate the phase locking value (PLV) to analyse the synchrony level between the areas. The PLV is given by
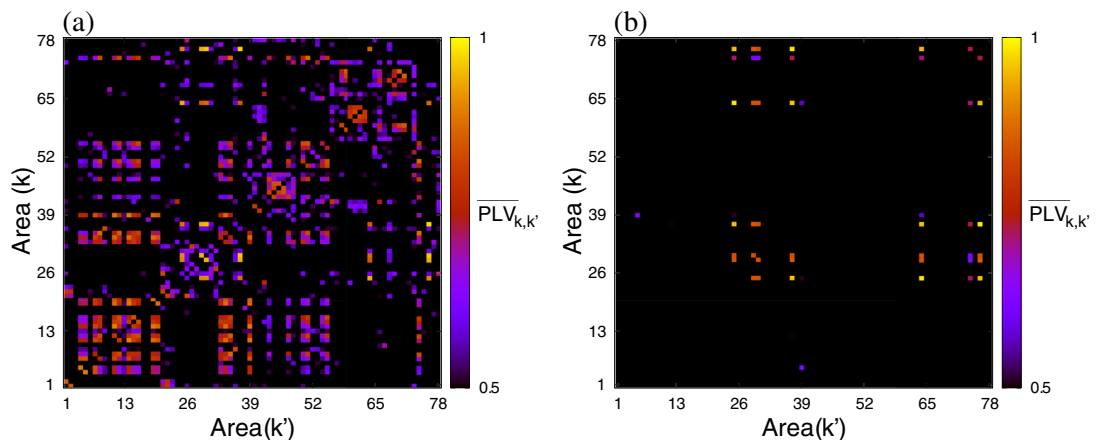
Figure 7. $\overline{PLV}_{k,k'}$ for $\varepsilon = 0.63$ and eight different initial conditions. We calculate the $\overline{PLV}_{k,k'}$ values for the areas with (a) $R > 0.5$ and (b) $R > 0.9$. The most interconnected areas 25, 29, 30, 37, 64, and 76 have $\overline{PLV}_{k,k'} > 0.8$.
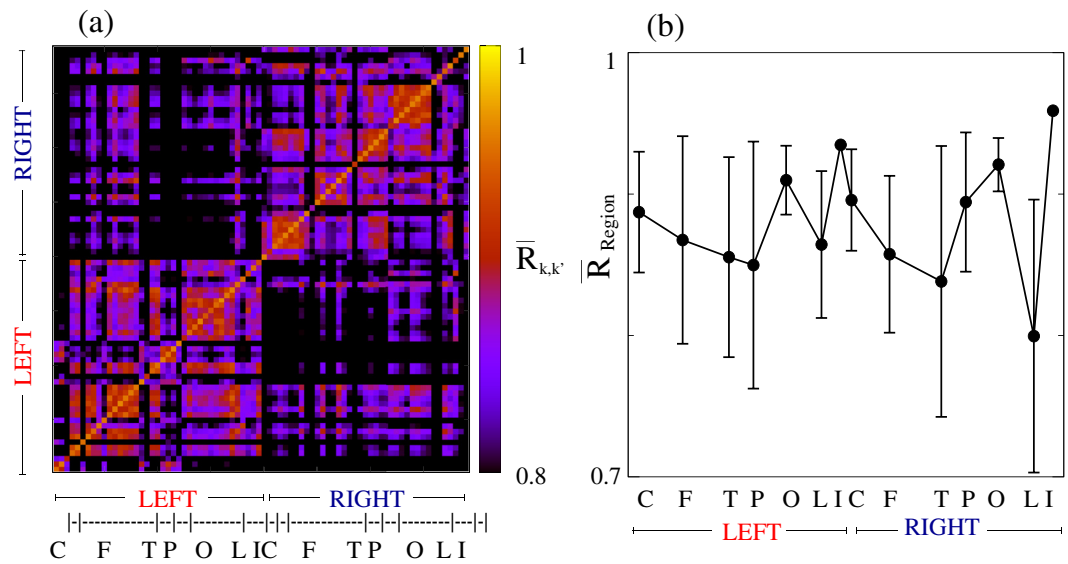

Figure 8. (a) $\bar{R}_{k,k'}$ for $\varepsilon = 0.7$ in the left and right hemispheres (C: central region, F: frontal, T: temporal, P: parietal, O: occipital, L: limbic, and I: insula). (b) $\bar{R}_{\text{Region}}$ for the cerebral regions, where the bars represent the standard deviation for eight different initial conditions.
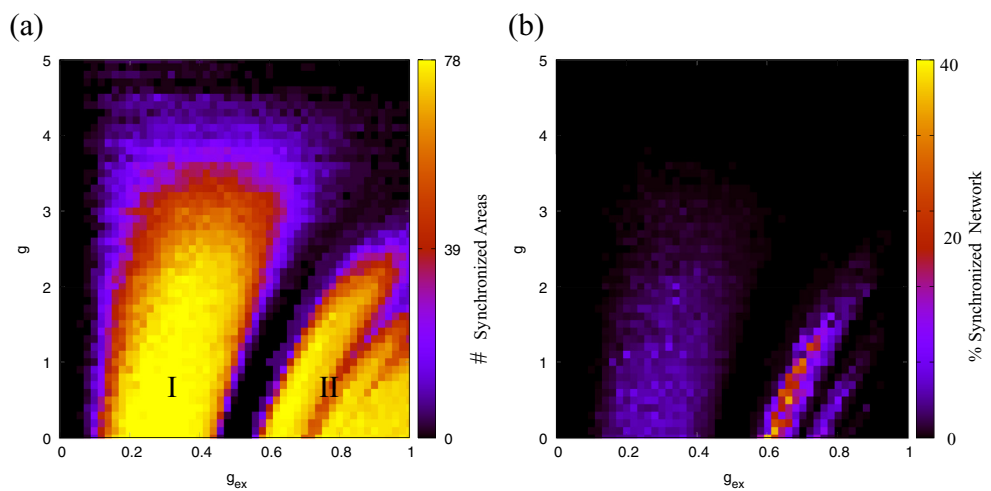

Figure 9. (a) Number of synchronised areas (colour bar) as a function of g_{ex} and g, where I and II denote spike and burst dynamics, respectively. (b) Percentage of synchronised areas among themselves in the network (colour bar) as a function of g_{ex} and g.

$$\mathrm{PLV}_{k,k'} = \frac{t_{\mathrm{step}}}{t_{\mathrm{final}} - t_{\mathrm{initial}}} \left| \sum_{t_{\mathrm{initial}}}^{t_{\mathrm{final}}} \mathrm{e}^{i\Theta_{k,k'}(t)} \right|, \tag{16}$$

where $\Theta_{k,k'}(t) = \Theta_k(t) - \Theta_{k'}(t)$ is the phase difference computed between the areas k and k' (Lachaux *et al* 1999, Lowet *et al* 2016). Figure 7 displays the mean of $\mathrm{PLV}_{k,k'}$ for different initial conditions. We verify that there are collective modes in the neuronal network. In figures 7(a) and (b), we calculate the $\overline{\mathrm{PLV}}_{k,k'}$ values for the areas with $R > 0.5$ and $R > 0.9$, respectively. We observe that the areas with burst synchronisation have the larger values of $\overline{\mathrm{PLV}}_{k,k'}$.

Figure 8(a) shows the cortico-cortical connection network, where the cortical areas are located in the left or right cerebral hemispheres. Each hemisphere is separated into regions: central (C), frontal (F), temporal (T), parietal (P), occipital (O), limbic (L), and insula (I). Considering $\varepsilon = 0.7$, as shown in figure 5(b), all subnetworks display burst dynamics and there are synchronous behaviours among neurons in the same subnetwork. We calculate the average order parameter of each region, given by

$$\bar{R}_{\mathrm{Region}} = \frac{1}{N_{\mathrm{Region}}} \sum_{k,k' \in I_{\mathrm{Region}}} \bar{R}_{k,k'}. \tag{17}$$

$\bar{R}_{\mathrm{Region}}$ is computed between the areas belonging to a set I_{Region} with N_{Region} areas, where I_{Region} corresponds to one region. By means of $\overline{R}_{\mathrm{Region}}$, we identify that the cortical areas in the occipital regions (O) are synchronised among themselves (figure 8(b)), due to the fact that these regions have areas with higher inter-connectivity than other regions and there are areas connected with highly connected neurons.

We plot the synchronisation patterns in the parameter space $g \times g_{\mathrm{ex}}$, where $g = g_{\mathrm{in}}/g_{\mathrm{ex}}$. Figure 9(a) displays the number of synchronised areas in colour scale as a function of g_{ex} and g. For $0.2 \lesssim g_{\mathrm{ex}} \lesssim 0.4$ and $g \lesssim 2$ all areas have synchronised spikes (region I), while for $g_{\mathrm{ex}} \gtrsim 0.6$ and $g \lesssim 2$ the areas present synchronised bursts (region II). There is a transition region (black) between spike and burst synchronisation, where all areas are desynchronised. In addition, synchronous behaviours for $g > 5$ are not observed, namely for g_{in} greater than $5g_{\mathrm{ex}}$. In figure 9(b), we plot the percentage of areas synchronised among themselves in the network. Our simulations show that the range of g_{ex} and g in which this percentage is large is narrow.

4. Conclusions

We have studied synchronisation in a neuronal network built according to the cortico-cortical connection network of the human brain. The network is composed of coupled random subnetworks with aEIF neurons. Depending on the control parameter, the aEIF neuron can spike or burst. In our network of networks we identify spike and burst synchronisation using as diagnostic tools CV and R.

We verify that the connectivity matrix has a rich-club organisation. There are six areas which are the most interconnected. They correspond to the rich-club elements and have many connections with other brain areas. Due to the particular properties of the chosen neuronal network model, the transition between desynchronised and synchronised patterns occurs first in the highly connected neurons. For small ε all areas have desynchronised spikes. Increasing ε, we observe that the areas pass through different synchronous behaviours according to the following sequence: (i) synchronised spikes, (ii) desynchronised spikes, (iii) burst synchronisation among the rich-club elements, and (iv) synchronised bursts. For large ε all areas show synchronised bursts, and the areas in the occipital region are synchronised among themselves. Liu *et al* (2015) reported that synchronous and desynchronous cortical activation can be associated with low δ-wave frequency during deep sleep and high frequency α-wave during quiet wake, respectively. They found different network dynamics of brainwave interactions in different brain areas during different sleep stages, as a result of interactions across brain locations.

We also show the influence of the relative inhibitory and excitatory conductance on synchronisation. In the parameter space $g \times g_{\mathrm{ex}}$ we find regions with spike and burst synchronisation, and a transition region characterised by areas with desynchronised spikes. In addition, no strong synchronisation is possible for $g_{\mathrm{in}} \gg g_{\mathrm{ex}}$. Large percentages of areas synchronised among themselves appear for few values of g_{in} and g_{ex}.

In future works we plan to analyse cluster synchronisation in our neuronal network model. Cluster synchronisation is characterised by different groups of neurons with distinct synchronous behaviours. Studies about cluster synchronisation have a physiological relevance due to the fact that this phenomenon can be associated not only with cognitive functions but also with long-range synchronisation.

Acknowledgments

ORCID iDs

R L Viana ⓘ https://orcid.org/0000-0001-7298-9370
F A S Ferrari ⓘ https://orcid.org/0000-0003-2534-5593

References

Andres D S, Gomez F, Ferrari F A S, Cerquetti D, Merello M, Viana R L and Stoop R 2014 Multiple-time-scale framework for understanding the progression of Parkinson's disease *Phys. Rev.* E **90** 062709

Bartsch R P, Liu K K L, Bashan A and Ivanov P C 2015 Network physiology: how organ systems dynamically interact *PLoS One* **10** e0142143

Bashan A, Bartsch R P, Kantelhardt J W, Havlin S and Ivanov P C 2012 Network physiology reveals relations between network topology and physiological function *Nat. Commun.* **3** 702

Borges F S, Protachevicz P R, Lameu E L, Bonetti R C, Iarosz K C, Caldas I L, Baptista M S and Batista A M 2017 Synchronised firing patterns in a random network of adaptive exponential integrate-and-fire neuron model *Neural Netw.* **90** 1–7

Brette R and Gerstner W 2005 Adaptive exponential integrate-and-fire model as an effective description of neuronal activity *J. Neurophysiol.* **94** 3637–42

Brown P 2003 Oscillatory nature of human basal ganglia activity: relationship to the pathophysiology of Parkinson's disease *Mov. Disord.* **18** 357–63

Bullmore E and Sporns O 2009 Complex brain networks: graph theoretical analysis of structural and functional systems *Nat. Rev. Neurosci.* **10** 186–98

Colizza V, Flammini A, Serrano M A and Vespignani A 2006 Detecting rich-club ordering in complex networks *Nat. Phys.* **2** 110–5

Connors B W and Gutnick M J 1990 Intrinsic firing patterns of diverse neocortical neurons *Trends Neurosci.* **13** 99–104

Deco G, Buehlmann A, Masquelier T and Hugues E 2011 The role of rhythmic neural synchronization in rest and task conditions *Front. Hum. Neurosci.* **5** 4

Erra R G, Velazquez J L P and Rosenblum M 2017 Neural synchronization from the perspective of non-linear dynamics *Front. Comput. Neurosci.* **11** 98

Fell J and Axmacher N 2011 The role of phase synchronization in memory processes *Nat. Rev. Neurosci.* **12** 105–18

Gabbiani F and Koch C 1998 Principles of spike train analysis *Methods in Neuronal Modeling: from Ions to Networks* 2nd edn, ed C Koch and I Segev (Cambridge, MA: MIT Press) 313–60

Gómez-Gardeñes J, Moreno Y and Arenas A 2007 Paths to synchronization on complex networks *Phys. Rev. Lett.* **98** 034101

Hagmann P, Cammoun L, Gigandet X, Meuli R, Honey C J, Wedeen V J and Sporns O 2008 Mapping the structural core of human cerebral cortex *PLoS Biol.* **6** e159

Ivanov P C and Bartsch R P 2014 Network physiology: mapping interactions between networks of physiologic networks *Networks of Networks: the Last Frontier of Complexity, Understanding Complex Systems* ed G D'Agostino and A Scala (Cham: Springer) pp 203–22

Ivanov P C, Liu K K L and Bartsch R P 2016 Focus on the emerging new fields of network physiology and network medicine *New J. Phys.* **18** 100201

Kuramoto Y 1984 *Chemical Oscillations, Waves and Turbulence* (New York: Springer)

Lachaux J P, Rodriguez E, Martinerie J and Varela F J 1999 Measuring phase synchrony in brain signals *Hum. Brain Mapp.* **8** 194–208

Liu K K L, Bartsch R P, Lin A, Mantegna R N and Ivanov P C 2015 Plasticity of brain wave network interactions and evolution across physiologic states *Front. Neural Circuits* **9** 62

Lo C-Y, Wang P-N, Chou K-H, Wang J, He Y and Lin C-P 2010 Diffusion tensor tractography reveals abnormal topological organization in structural cortical networks in Alzheimer's disease *J. Neurosci.* **30** 16876–85

Lowet E, Roberts M J, Bonizzi P, Karel J and De Weerd P 2016 Quantifying neural oscillatory synchronization: a comparison between spectral coherence and phase-locking value approaches *PLoS One* **11** e0146443

Naud R, Marcille N, Clopath C and Gerstner W 2008 Firing patterns in the adaptive exponential integrate-and-fire model *Biol. Cybern.* **99** 335–47

Noback C R, Strominger N L, Demarest R J and Ruggiero D A 2005 *The Human Nervous System: Structure and Function* (Totowa, NJ: Humana Press)

Opsahl T, Colizza V, Panzarasa P and Ramasco J J 2008 Prominence and control: the weighted rich-club effect *Phys. Rev. Lett.* **101** 168702

Ottersen O P and Storm-Mathisen J 1986 Excitatory amino acid pathways in the brain *Adv. Exp. Med. Biol.* **203** 263–84

Pikovsky A, Rosenblum M and Kurths J 2001 *Synchronization: a Universal Concept in Nonlinear Sciences* (Cambridge: Cambridge University Press)

Rodriguez E, George N, Lachaux J P, Martinerie J, Renault B and Varela F J 1999 Perception's shadow: long-distance synchronization of human brain activity *Nature* **397** 430–3

Shaw P *et al* 2008 Neurodevelopmental trajectories of the human cerebral cortex *J. Neurosci.* **28** 3586–94

Tallon-Baudry C 2009 The roles of gamma-band oscillatory synchrony in human visual cognition *Front. Biosci.* **14** 321–32

Touboul J and Brette R 2008 Dynamics and bifurcations of the adaptive exponential integrate-and-fire model *Biol. Cybern.* **99** 319–34

Traub R D and Wong R K 1982 Cellular mechanism of neuronal synchronization in epilepsy *Science* **216** 745–7

Uhlhaas P J and Singer W 2006 Neural synchrony in brain disorders: relevance for cognitive dysfunctions and pathophysiology *Neuron* **52** 155–68

van den Heuvel M and Sporns O 2011 Rich-club organization of the human connectome *J. Neurosci.* **31** 15775–86

Zhang X, Boccaletti S, Guan S and Liu Z 2015 Explosive synchronization in adaptive and multilayer networks *Phys. Rev. Lett.* **114** 038701

Zhang X, Zou Y, Boccaletti S and Liu Z 2014 Explosive synchronization as a process of explosive percolation in dynamical phase space *Sci. Rep.* **4** 5200